

Transfer-Learned Potential Energy Surfaces: Towards Microsecond-Scale Molecular Dynamics Simulations in the Gas Phase at CCSD(T) Quality

Silvan Käser and Markus Meuwly*

*Department of Chemistry, University of Basel, Klingelbergstrasse 80 , CH-4056 Basel,
Switzerland.*

E-mail: m.meuwly@unibas.ch

March 22, 2023

Abstract

The rise of machine learning has greatly influenced the field of computational chemistry, and that of atomistic molecular dynamics simulations in particular. One of its most exciting prospects is the development of accurate, full-dimensional potential energy surfaces (PESs) for molecules and clusters, which, however, often require thousands to tens of thousands of *ab initio* data points restricting the community to medium sized molecules and/or lower levels of theory (e.g. DFT). Transfer learning, which improves a global PES from a lower to a higher level of theory, offers a data efficient alternative requiring only a fraction of the high level data (on the order of 100 are found to be sufficient for malonaldehyde). The present work demonstrates that even with Hartree-Fock theory and a double-zeta basis set as the lower level model, transfer learning yields CCSD(T)-level quality for H-transfer barrier energies, harmonic frequencies and H-transfer tunneling splittings. Most importantly, finite-temperature molecular dynamics simulations on the sub- μ s time scale in the gas phase are possible and the infrared spectra determined from the transfer learned PESs are in good agreement with experiment. It is concluded that routine, long-time atomistic simulations on PESs fulfilling CCSD(T)-standards become possible.

1 Introduction

Over the past decade, machine learning-based approaches have persistently influenced the field of computational chemistry as a whole and that of atomistic molecular dynamics (MD) simulations in particular.¹⁻³ Machine learning (ML) approaches begin to be routinely used in areas ranging from reaction planning,^{4,5} to drug design^{6,7} and to the construction and use of accurate local and global potential energy surfaces (PESs).^{3,8-10} Common to all these applications is that they are data-driven, i.e. they depend on the amount but also on the quality of the available data on which the statistical models are trained. With respect to the underlying

ing models themselves, much flexibility exists, encompassing kernel- or neural network-based approaches with a wide range of architectures and specific design choices.^{2,3,8,9,11}

The construction of a multidimensional PES suitable for routine and robust MD simulations remains a challenging task.¹² An established approach consists of precomputing reference energies and forces from electronic structure methods at suitable and affordable levels of theory for a given molecule or system, also often with particular applications such as various spectroscopies or reaction dynamics in mind. Traditionally, these energies were used to fit predetermined parametrized forms which in turn not only provide the total energy of the system but also analytical derivatives for forces required in MD simulations. The difficulty in such approaches consists in “guessing” sufficiently flexible forms of the parametrization to capture local and global features of the PES alike. Also, such parametrized fits are often highly nonlinear which is another challenge, in particular for high-dimensional PESs.

ML methods, including (reproducing) kernel^{13,14} or neural network (NN) approaches,^{15,16} have been long known to be flexible function approximators.¹⁷ It is precisely this flexibility that is also beneficial for the representation of molecular PESs which can have a wide range of topographies and designing parametrizations suitable for capturing all relevant features becomes increasingly difficult.

Here, the construction, improvement and use of reactive PESs in ring-polymer instanton (RPI) calculations and MD simulations is discussed with the purpose of illustrating practical aspects and probing the quality of the resulting surfaces. The method employed to improve PESs from a lower level (LL) to a higher level (HL) of theory is transfer learning (TL)^{18–20} which is rooted in the notion that the overall topographies of molecular PESs at different levels of theory are often similar. As an example, it is often found that the number of local minima is comparable or even identical if quantum chemical methods at different

levels of theory are employed, whereas the geometrical structures of course differ. This topographical similarity can be exploited in TL approaches in that measured amounts of HL information are used to locally distort the model based on LL data. One particular focus in the present work is on studying the influence of the level of electronic structure theory used to construct the surrogate LL model on the quality of the HL PES and making best use of the data generated. To the best of our knowledge this contribution presents the first systematic analysis of the influence of the LL PES in TL of global reactive molecular potential energy surfaces.

Malonaldehyde (MA) is a well-studied molecule experimentally²¹⁻²⁸ and from computations²⁹⁻³³ and provides a suitable benchmark system for the present work and recent results³⁴ serve as a reference. The properties used for evaluating the quality of the final PESs include energies (e.g. RMSE(E) from comparison to *ab initio* reference), barrier heights for hydrogen transfer (H-transfer), harmonic frequencies ω (allowing comparison with experiments^{25,35} and *ab initio* results³⁴), and tunneling splittings $\Delta_{\text{H/D}}$ (allowing comparison to experiment²¹⁻²³ and literature³⁴). Alternative/additional observables include H-transfer rates and infrared spectra inferred from MD simulations which can also be compared with experiment.

The present work is structured as follows. First, the methods including the NN-based representation of the PESs and TL are discussed. Then, the results comprising out of sample errors, energy barriers, harmonic frequencies and tunneling splittings as well as the results from an aggregate of 1.5 μs of MD simulations are presented. Finally, the results are discussed in a broader context and compared to previous experiments and computational work.

2 Methods

This section introduces the employed ML approaches, the data generation procedure, RPI theory, the MD simulation protocol, analysis and computation of the observables.

2.1 Machine Learning

All full-dimensional, reactive PESs used in this work are represented by a high dimensional, message-passing³⁶ NN of the PhysNet type.¹⁵ PhysNet predicts energies, forces and dipole moments for arbitrary molecular configurations from a feature vector that is learned to describe the local chemical environment (here, up to a cutoff radius $r_{\text{cut}} = 10 \text{ \AA}$) of each atom i . The total potential energy of a molecule with N atoms for a given geometry is given by

$$E = \sum_{i=1}^N E_i + k_e \sum_{i=1}^N \sum_{j>i}^N \frac{q_i q_j}{r_{ij}} \quad (1)$$

where E_i are the atomic contributions to the total energy of the molecule, k_e is Coulomb’s constant and the second term describes pairwise electrostatic contributions. Note that the partial charges q_i are corrected for charge conservation and that the electrostatic contribution is damped at small inter-atomic distances r_{ij} due to the singularity (for details see Reference 15). The forces \mathbf{F} and Hessians \mathbf{H} are obtained analytically from reverse mode automatic differentiation³⁷ as implemented in Tensorflow³⁸ and the dipole moment is calculated as

$$\boldsymbol{\mu} = \sum_{i=1}^N q_i \mathbf{r}_i. \quad (2)$$

The learnable parameters in PhysNet were fit to reference *ab initio* energies, forces and dipole moments following the procedure described in Reference 15. Note that the partial charges q_i were adapted to best reproduce the dipole moment from the *ab initio* calculations.

Recently, TL^{20,39} and related approaches including Δ -ML⁴⁰⁻⁴² have become very popular and successful in improving a given LL PES to a HL of theory. At its core, TL builds on the knowledge acquired by solving one task (representing the LL PES) to solve a new, related task (representing the HL PES).²⁰ In practice, the parameters of the LL PES are used as a good initial guess and are fine-tuned with little, though judiciously, chosen HL information. In this work, all parameters of PhysNet were allowed to change in the TL step.

2.2 *Ab Initio* Data

All molecular structures that were used to in the fitting procedure of PhysNet were available from earlier work³³ and their sampling process is described in detail in Reference 33. The data set contains structures for MA, acetoacetaldehyde (3-oxobutanal), acetylacetone (pentan-2, 4-dion) as well as a total of 49 substructures as motivated by the "amon" approach.⁴³ An initial set of structures was generated by running Langevin dynamics at 1000 K using the semi-empirical PM7 method⁴⁴ as implemented in MOPAC.⁴⁵ Next, *ab initio* energies, forces and dipole moments were determined at the MP2/aug-cc-pVTZ (aVTZ) level of theory using MOLPRO⁴⁶ and were used to train two preliminary PhysNet models. The preliminary models were then used to suitably augment the data set using adaptive sampling.⁴⁷ The final data set contained MP2/aVTZ level energies, forces and molecular dipole moments for a total of 71 208 structures including all three molecules and their amons. This PES is referred to as PhysNet^{MP2}.

To be able to study the influence of the LL on the quality of the HL, the data set containing 71 208 structures from earlier work³³ was recalculated at two additional "low" levels of theory, namely HF/cc-pVDZ (VDZ) and B3LYP/aVTZ using MOLPRO.⁴⁶ The two new data sets are used to learn representations of the PES using PhysNet and are termed PhysNet^{HF} and PhysNet^{B3LYP}, respectively. The relative CPU times for the *ab initio* calculations (that include energies, forces and dipole moments) are roughly 1:10:170:4000 for the HF/VDZ,

B3LYP/aVTZ, MP2/aVTZ and CCSD(T)/aVTZ levels of theory, respectively.

The CCSD(T)/aVTZ level of theory was chosen as higher level of theory, which is computationally much more demanding, and will serve as target in the TL step.³⁴ Although the determination of forces and dipole moments is roughly an order of magnitude more expensive than an energy-only calculation, the information gained from including gradients (27 components for malonaldehyde) and dipole moments is considerable. The data set sizes employed in the TL step of the present work include $N = [25, 50, 100, 862]$ (corresponding to TL₀, TL₁, TL₂ and TL_{ext}) MA structures. Except for $N = 862$ (which corresponds to an extended data set that contains all HL information.³⁴) the MA structures were augmented iteratively and are specifically chosen to ideally cover all relevant spatial regions (i.e. structures on and around the minimum energy path, instanton path, global minimum and transition state) of the PESs that were found to be important for the determination of the tunneling splitting.³⁴ The resulting TL PESs corresponding to the LL models (PhysNet^{HF}, PhysNet^{B3LYP} or PhysNet^{MP2}) are termed TL_y^x with $x \in [\text{HF}, \text{B3LYP}, \text{MP2}]$ and $y \in [0, 1, 2, \text{ext}]$.

2.3 Ring-Polymer Instanton Theory

The ring polymer instanton (RPI) method offers a semiclassical approximation for computing tunneling splittings in molecular systems.^{48–51} Instanton theory, which is closely related to the WKB approximation⁵² in a one-dimensional model can be applied to multidimensional systems as well. It identifies the optimal tunneling pathway, called the instanton, by locating the imaginary-time $\tau \rightarrow \infty$ path connecting two degenerate wells that minimizes the action, S . To determine the instanton, a ring-polymer optimization technique is used to discretize the path into N beads and take the limit as $N \rightarrow \infty$. S is then determined using information from the potential energy of and distances between neighboring beads along the instanton path (IP). Usually, the instanton path does not pass through the saddle point of the reaction

and is different from the minimum energy path. In addition to the IP, a contribution Φ characterizing the fluctuations around the path needs to be computed to second order which necessitates the availability of Hessians at each bead. The tunneling splitting is then given by

$$\Delta = \frac{2\hbar}{\Phi} \sqrt{\frac{S}{2\pi\hbar}} e^{-S/\hbar}. \quad (3)$$

Full technical details regarding the RPI approach are given, e.g., in References 53 and 54.

2.4 Molecular Dynamics Simulations

The MD simulations evaluated in this work were all performed using PhysNet PESs and using the atomic simulation environment (ASE⁵⁵) in Python. Starting from a given PES, the structure of MA was first optimized to its minimum energy structure before random momenta were drawn from a Maxwell-Boltzmann distribution corresponding to $T = [300, 500]$ K and assigned to the atoms. The MD simulations were carried out in the *NVE* ensemble using the Velocity Verlet algorithm and a time step of $\Delta t = 0.25$ fs to conserve energy as bonds involving hydrogen were flexible. The system was first allowed to equilibrate for 2.5 ps and was followed by a production simulation of 250 ps each. At each temperature and using a representative HL PES for each class of TL PESs, 1000 independent trajectories were run using different initial momenta. This accumulated to a total of 750 ns simulation time per temperature T .

The MD simulations were used to estimate H-transfer rates, which were calculated as the accumulated number of H-transfers divided by the accumulated total simulation time, $N_{\text{HT}}/t_{\text{tot}}$. A H-transfer was considered complete whenever the H-atom transfers from being closer to one O-Atom to the other (e.g. when $r_{\text{O}_\text{A}\text{H}} < r_{\text{O}_\text{B}\text{H}}$ changes to $r_{\text{O}_\text{A}\text{H}} > r_{\text{O}_\text{B}\text{H}}$), although other

criteria exist and have been used.⁵⁶ For the present work the details of the criterion are of less interest because only the relative rates from simulation based on the different PESs is analyzed. The same trajectories were also used to compute infrared (IR) spectra from the Fourier transform of the dipole-dipole auto-correlation function,⁵⁷ according to

$$I(\omega)n(\omega) \propto Q(\omega) \cdot \text{Im} \int_0^\infty dt e^{i\omega t} \sum_{i=x,y,z} \langle \boldsymbol{\mu}_i(t) \cdot \boldsymbol{\mu}_i(0) \rangle. \quad (4)$$

Here, the Fourier transform was further corrected by a quantum correction factor⁵⁸ $Q(\omega) = \tanh(\beta\hbar\omega/2)$.

3 Results

The following section presents first the results derived from the LL PESs for MA. This includes out of sample errors, energy barriers and harmonic frequencies as determined from the LL PESs including the comparison to their *ab initio* references, and tunneling splittings. This is followed by the results for the HL PESs.

3.1 Quality of LL PESs

The LL PESs generated at three different levels of theory including HF, B3LYP and MP2 (PhysNet^{HF}, PhysNet^{B3LYP} and PhysNet^{MP2}) are evaluated on a test set containing 9208 structures. The mean absolute (MAE) and root mean squared (RMSE) errors on energies and forces are summarized in Table 1. MAE(E) for all models are below 0.05 kcal/mol and are lowest for PhysNet^{MP2} (0.02 kcal/mol). Conversely, the RMSE(E) for PhysNet^{MP2} is highest (a factor of ~ 5 larger than for PhysNet^{HF} and PhysNet^{B3LYP}). The MAE(F) are within 0.008 kcal/mol/Å for all three LL PESs while the RMSE(F) differ by ~ 0.1 kcal/mol/Å at most. The correlation and the errors of the PhysNet energies with respect to the respective

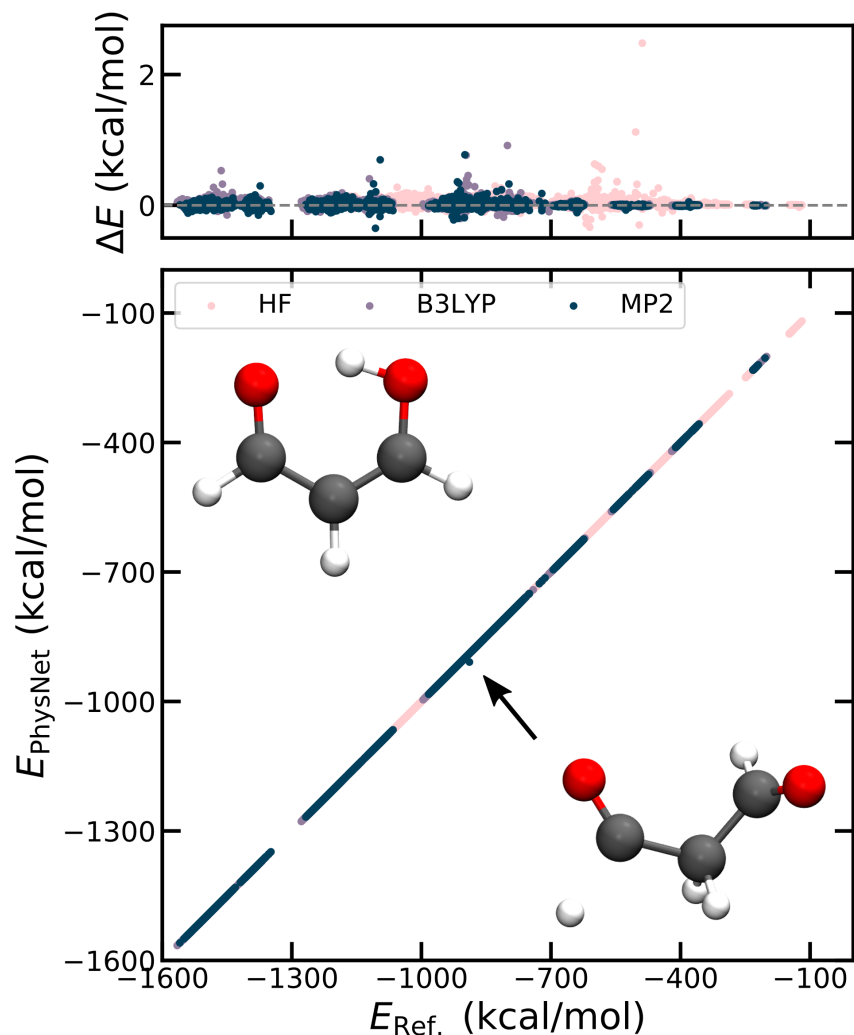


Figure 1: The main panel shows the out of sample performance of the LL models. PhysNet models are trained on energies, forces and dipole moments determined at the HF/VDZ, B3LYP/aVTZ and MP2/aVTZ level of theory for a total 71 208 structures. 9208 structures ($\sim 13\%$) served as test set and were not used during training. The test set contains structures for MA, acetoacetaldehyde, acetylacetone and the amons. The top panel reports $\Delta = E_{\text{Ref.}} - E_{\text{PhysNet}}$ and contains all but a single outlier from the MP2 model (that has $\Delta \approx 20$ kcal/mol) and is shown in the lower right corner of the main panel at ~ -800 kcal/mol) which was omitted for better visibility of the errors. The molecular structure in the upper left corner shows the global minimum of MA.

reference *ab initio* values are shown in Figure 1 for the test set.

The barrier for H-transfer from the *ab initio* calculations varied between 9.96, to 2.98 and 2.74 kcal/mol for the HF, B3LYP and MP2 level of theory, respectively. Excellent fitting

accuracy with respect to *ab initio* reference is found for all LL PESs with the largest absolute deviation of 0.05 kcal/mol for PhysNet^{MP2}. These barrier heights compare with 4.03 kcal/mol and 4.09 kcal/mol from high-level CCSD(T) calculations of different flavours.^{8,31}

Harmonic frequencies constitute an additional measure for the accuracy of a PES around a stationary point. The MAEs and the RMSEs for the harmonic frequencies of the global minimum of MA for all LL PESs are reported in Table 1. While the MAEs (RMSEs) for all LL PESs are below 5 (7) cm⁻¹, the errors for PhysNet^{HF} are slightly larger by approximately a factor of 2 compared to PhysNet^{B3LYP} and PhysNet^{MP2}, which are within 0.1 cm⁻¹ of one another. The actual deviation of the PhysNet harmonic frequencies with respect to their reference is shown in Figure 2 for the global minimum of MA. The largest difference is found for PhysNet^{HF} with a deviation of ~ 17 cm⁻¹. For the H-transfer transition state, the MAEs (RMSEs) are all below 6 (9) cm⁻¹ (see Table S2). Here, PhysNet^{B3LYP} yields the most accurate frequencies with a MAE and RMSE of 2.3 and 3.6 cm⁻¹, respectively. A comprehensive list of the harmonic frequencies for the minimum and H-transfer transition state as calculated on the LL PhysNet PESs and their *ab initio* reference are given in Tables S1 and S2, respectively.

As one of the target observables, that allows a comparison to experiment,²¹⁻²³ the tunneling splittings for H-transfer and deuterium transfer (D-transfer) $\Delta_{\text{H/D}}$ are calculated for all LL PESs. The tunneling splitting is exquisitely sensitive to the quality and accuracy of the PES along and around the instanton path comprising the minimum energy structure and the region near the transition state. The tunneling splitting for H-transfer, Δ_{H} , ranges from 0.036, to 71.1 and to 96.3 cm⁻¹ for PhysNet^{HF}, PhysNet^{B3LYP} and PhysNet^{MP2}. Similarly, the tunneling splittings for D-transfer, Δ_{D} , are $9.9 \cdot 10^{-4}$, 12.8 and 18.8 cm⁻¹. This compares with experimentally^{21,22} determined tunneling splittings of 21.583 and 2.915 cm⁻¹ for H-transfer and D-transfer, respectively, and RPI calculations at CCSD(T) quality (TL +

RPI)³⁴ of 25.3/3.7 cm⁻¹. The hydrogen tunneling splitting Δ_{H} spans more than three orders of magnitude and impressively illustrates its exquisite sensitivity to the shape and accuracy of the PES.

Table 1: Summary of the performance of the LL PhysNet PESs: Out of sample errors for predicting the test set of 9208 structures for which energies and forces have been determined at the three different levels of theory. Energy barrier E_{B} for H-transfer obtained from PhysNet and from *ab initio* calculations $E_{\text{B}}^{\text{Ref.}}$. MAEs and RMSEs for harmonic frequencies obtained from the LL PES with respect to appropriate reference *ab initio* frequencies. Tunneling splittings for H-transfer and D-transfer obtained from PhysNet Δ are listed. The experimentally^{21,22} determined tunneling splitting is 21.583 and 2.915 cm⁻¹ for H-transfer and D-transfer, respectively, which compares to CCSD(T) quality predictions (TL + RPI)³⁴ of 25.3/3.7 cm⁻¹.

	HF	B3LYP	MP2
MAE(E)/(kcal/mol)	0.046	0.028	0.020
RMSE(E)/(kcal/mol)	0.063	0.040	0.210
MAE(F)/(kcal/mol/Å)	0.067	0.059	0.062
RMSE(F)/(kcal/mol/Å)	0.177	0.141	0.242
E_{B} /(kcal/mol)	10.00	3.02	2.79
$E_{\text{B}}^{\text{Ref.}}$ /(kcal/mol)	9.96	2.98	2.74
MAE(ω)/(cm ⁻¹)	4.8	2.6	2.5
RMSE(ω)/(cm ⁻¹)	6.2	3.5	3.6
Δ_{H} /(cm ⁻¹)	0.0358	71.1	96.3
Δ_{D} /(cm ⁻¹)	0.000991	12.8	18.8

3.2 Performance of the TL PESs

The quality of the HL, transfer-learned PESs TL_y^x with $x \in [\text{HF}, \text{B3LYP}, \text{MP2}]$ and $y \in [0, 1, 2, \text{ext}]$ starting from three different LL PESs is broadly evaluated next. On account of the small HL data set sizes (including $N = [25, 50, 100, 862]$ for TL₀, TL₁, TL₂ and TL_{ext}), each TL is repeated 10 times on different splits of the data. The energy barriers E_{B} for the different HL PESs together with their variation are shown in Figure 3 for all TLs (transparent circles). Their averages and standard deviations are indicated as opaque circles and error bars,

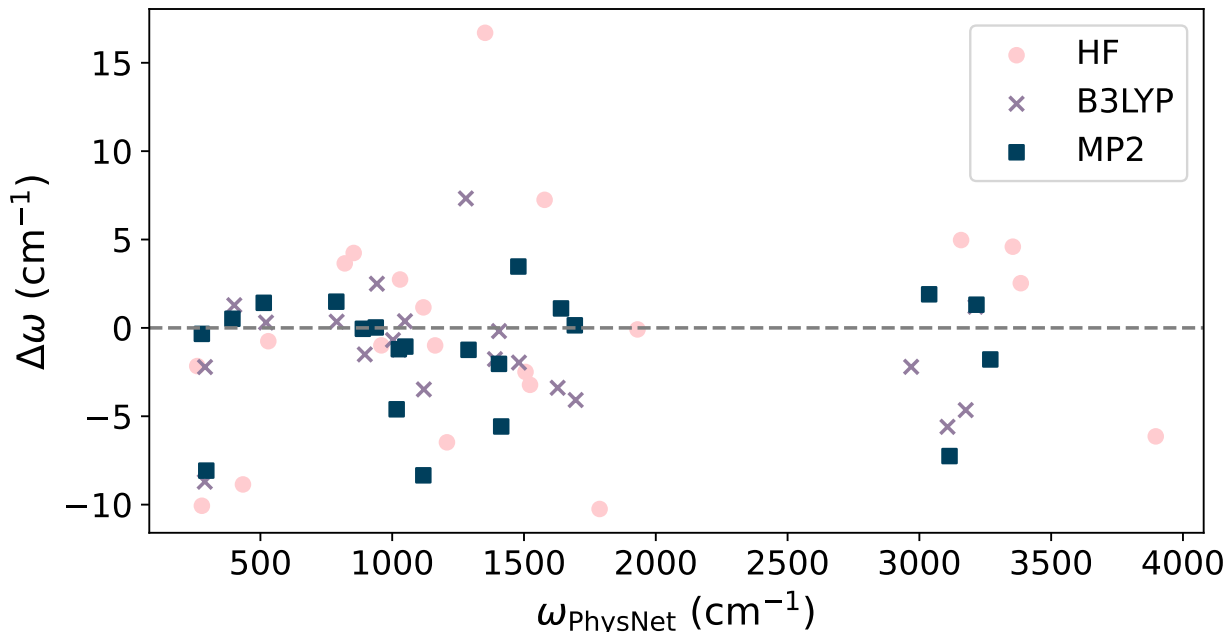


Figure 2: Harmonic frequencies ω of MA together with their representation errors $\Delta\omega = \omega_{\text{Ref.}} - \omega_{\text{PhysNet}}$ determined from PhysNet trained on reference data at the LL methods. A corresponding plot for the frequencies of the H-transfer transition state is given in Figure S1 and all harmonic frequencies are listed in Tables S1 and S2.

respectively. The gray dashed line corresponds to the *ab initio* CCSD(T)/aVTZ energy barrier determined in previous work.³⁴ While $\text{TL}_0^{\text{B3LYP}}$ and TL_0^{MP2} (i.e. requiring only 25 data points) already yield E_B within 0.003 kcal/mol of the *ab initio* CCSD(T)/aVTZ barrier, the deviation of ~ 0.06 kcal/mol for TL_0^{HF} is slightly larger. For all larger data set sizes, the energy barrier for H-transfer of the HL PESs are accurate and equal among themselves to within ~ 0.01 kcal/mol. Overall, TL from all LL models yields HL models with E_B for H-transfer to within 0.06 kcal/mol of the reference value from *ab initio* CCSD(T)/aVTZ calculations determined in previous work.³⁴ This *ab initio* CCSD(T)/aVTZ barrier of 3.895 kcal/mol compares to values of 4.09 and 4.03 kcal/mol as obtained at the CCSD(T)/aug-cc-pV5Z (optimization carried out at CCSD(T)/aVTZ level) and fc-CCSD(T) (F12*)/def2-TZVPP level of theory, respectively.^{8,31}

The energy barrier E_B for H-transfer is a local, rather low dimensional property of a PES.

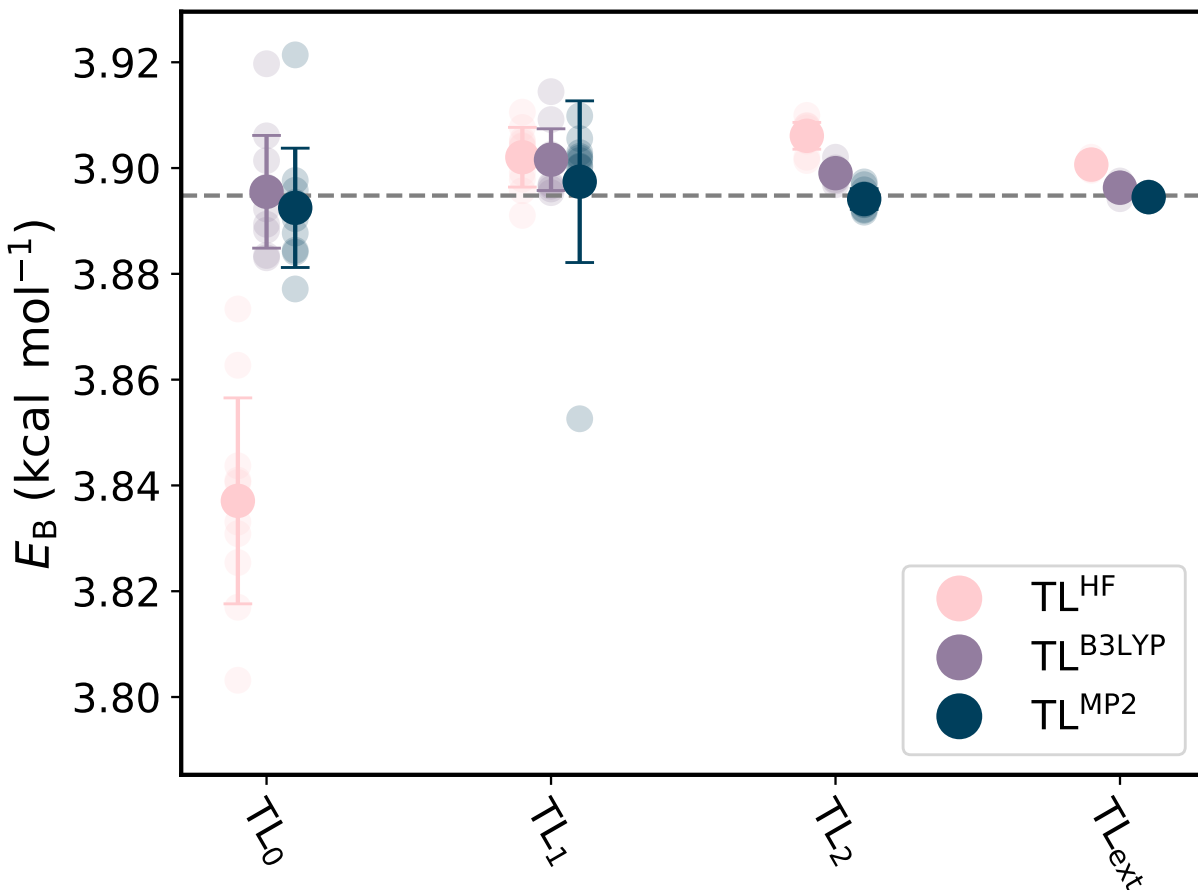


Figure 3: Energy barriers E_B for H-transfer from all TL PESs (transparent circles). The corresponding averages (opaque circle) and standard deviations (error bars as $\pm\sigma$) are indicated as well. The different colors represent TLs that were started based on LL PESs of different levels of theory, including HF, B3LYP and MP2. The gray dashed line corresponds to the *ab initio* barrier height for H-transfer at the CCSD(T)/aug-cc-pVTZ level of theory and is $E_B = 3.8948$ kcal/mol. The energy barriers are accurate already for TL₀ (25 data points), except for TL^{HF}. Presumably, this is caused by the rather big difference between the HF and the (target) CCSD(T) energy barrier.

Conversely, harmonic frequencies for stationary points probe the curvature of the PES in all directions. Figure 4 shows the MAE and RMSEs of ensemble predictions (i.e. an average over 10 TLs) for the global minimum of MA of TL^{HF}, TL^{B3LYP} and TL^{MP2} for the different TL data set sizes (i.e. 25, 50, 100, 862). Averaged errors below 6 cm⁻¹ are achieved for all HL PESs with as little as 25 data points. TL with 100 CCSD(T)/aVTZ data points the MAEs (RMSEs) are further reduced to 2.4, 1.3 and 1.5 (3.4, 1.8 and 2.0) cm⁻¹ for TL₂^{HF},

TL_2^{B3LYP} and TL_2^{MP2} , respectively. The RMSEs between the *ab initio* HF/B3LYP/MP2 harmonic frequencies and the high-level CCSD(T) frequencies are 177, 28 and 21 cm^{-1} for HF, B3LYP and MP2, respectively, and provides an impression by how much the shape of the LL PESs need to adjust around the minimum at the TL step.

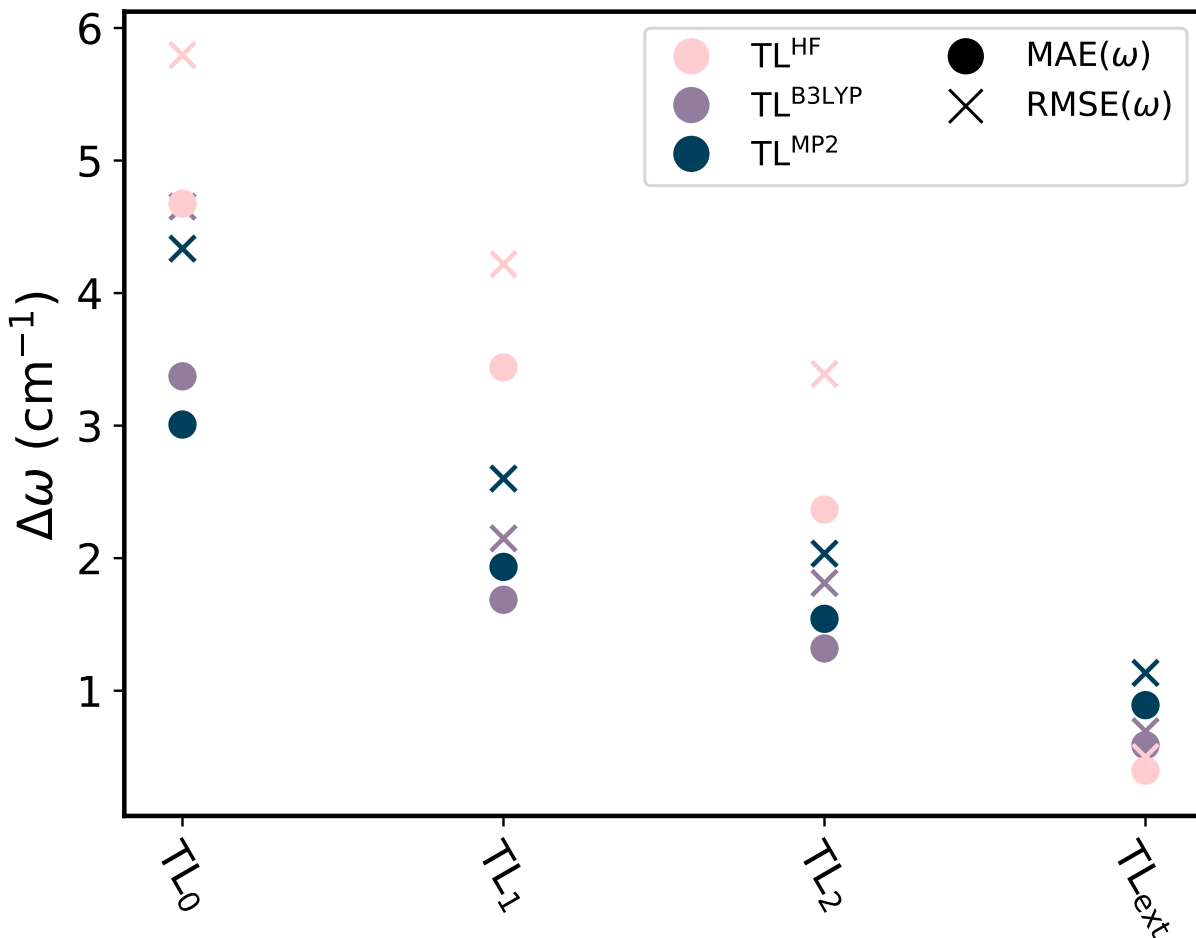


Figure 4: The ensemble prediction of harmonic frequencies for the optimized structure of MA obtained from the different TL_y ($y \in [0, 1, 2, \text{ext}]$) models are compared to the reference harmonic frequencies calculated at the CCSD(T)/aVTZ level of theory. Mean absolute errors (MAE) and root mean squared errors (RMSE) are reported. The "null hypothesis" (i.e. the RMSE of the *ab initio* HF/B3LYP/MP2 harmonic frequencies with respect to the CCSD(T) frequencies) yields an RMSE of 177, 28 and 21 cm^{-1} for HF, B3LYP and MP2, respectively.

The tunneling splitting is sensitive to the local dynamics and the PES's topology around the H-transfer instanton path. Hydrogen and deuterium tunneling splittings were used as target

observables in recent work for the iterative and systematic construction of different data sets based on PhysNet^{MP2}.³⁴ Figure 5 presents the tunneling splittings for H-transfer and D-transfer as calculated from all different HL PESs (TL₀^{HF} to TL_{ext}^{MP2}). Again, their averages and standard deviations are shown as opaque circles and error bars, respectively. As had been found for E_B , the fluctuation is largest for TL₀^{HF} with tunneling splittings ranging from ~ 18 to 42 cm^{-1} . This fluctuation is smaller by a factor of ~ 5 for both TL₀^{B3LYP} and TL₀^{MP2}. For TL₂ the fluctuation among the three classes of HL PES become comparable. Average Δ_H of 20.7, 22.9 and 25.2 cm^{-1} are found for TL₂^{HF}, TL₂^{B3LYP} and TL₂^{MP2}. Increasing the data set size to 862 (TL_{ext}) further reduces both the differences within the classes and the standard deviation of the ensemble predictions. Here, average Δ_H of 23.2, 23.9 and 25.3 cm^{-1} are found for TL_{ext}^{HF}, TL_{ext}^{B3LYP} and TL_{ext}^{MP2}, respectively. It is noted, that Δ_H from TL^{MP2} only marginally changed upon increasing the TL data set size from 100 to 862 (TL₂ to TL_{ext}). Similar observations hold for D-transfer, which indicates that TL₂^{MP2} is basically converged with MP2 as the LL model.

3.3 Molecular Dynamics on the HL PESs

Further evaluations focus on dynamical properties derived from MD simulations carried out on the HL PESs. As a TL data set size of 100 CCSD(T) data points (TL₂) is a very realistic scenario for final predictions (i.e. allows to check for convergence of the results and a small enough data set size to be amenable also for larger systems), a representative PES (from the 10 independent TL executions) was chosen for each of the three TL classes (i.e. TL₂^{HF}, TL₂^{B3LYP} and TL₂^{MP2}).

H-transfer rates obtained from *counting* H-transfers and dividing by total simulation time from the MD simulations at 300 and 500 K are reported in Table 2. The rates at both temperatures agree to approximately 30 % and correspond to ~ 1 (34) transfers per ns at

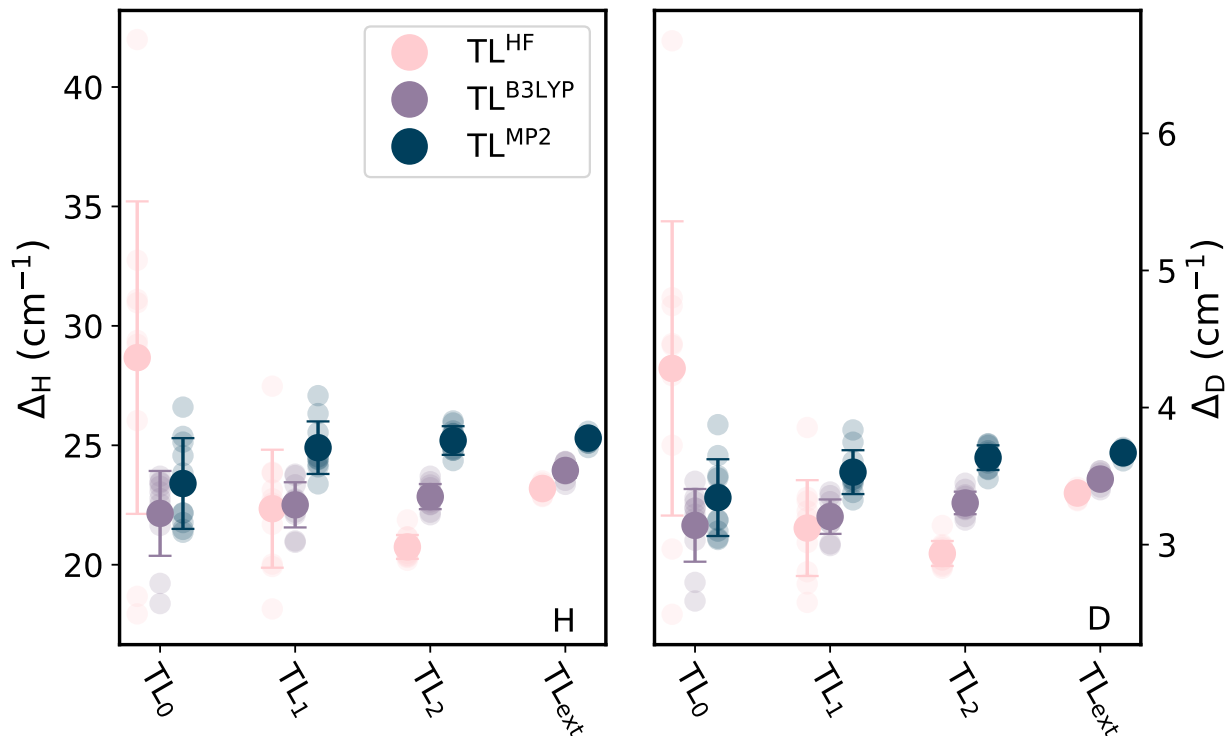


Figure 5: Tunneling splittings for H- and D-transfer (left and right panels) from all TL PESs (transparent circles). The corresponding averages (opaque circle) and standard deviations (error bars as $\pm\sigma$) are indicated as well. The different colors represent TLs that were started based on LL PESs of different levels of theory, including HF, B3LYP and MP2.

300 (500) K. It is interesting to note that the trend at 300 K (i.e. lowest rate for TL^{HF} followed by L^{B3LYP} and TL^{MP2}) reverses at 500 K. Overall, the rates for TL^{B3LYP} and TL^{MP2} are more similar to one another.

The simulation run at 300 K were further used to compute IR spectra as calculated from the dipole-dipole autocorrelation function, see Figure 6 (middle panel) for TL_2^{HF} , $\text{TL}_2^{\text{B3LYP}}$ and TL_2^{MP2} . As additional reference, an IR spectrum was also calculated on $\text{TL}_{\text{ext}}^{\text{MP2}}$ which, starting from the MP2 LL PES, has been trained on an extended TL data set containing 862 CCSD(T) data points and is thus expected to yield results closest to simulations on a - hypothetical - PhysNet PES trained on CCSD(T)/aVTZ reference data. The spectra derived from the dynamics on the HL PESs are very similar with one another. Single deviations can,

Table 2: H-transfer rates (in ns⁻¹) obtained from running MD simulations using representative HL PESs. The *NVE* simulations are initialized with random momenta drawn from a Maxwell-Boltzmann distribution corresponding to 300 and 500 K, respectively. Each rate is obtained from an aggregate of 250 ns (1.5 μ s in total).

(1/ns)	300 K	500 K
TL ^{HF}	0.9	41.0
TL ^{B3LYP}	1.1	32.1
TL ^{MP2}	1.4	33.9

e.g. be found at ~ 230 cm⁻¹ or at ~ 1650 cm⁻¹, where TL₂^{HF} has no or only a small fraction of the intensity in comparison to the other spectra, respectively. The difference spectra $\Delta I(\nu) = I_{TL_{\text{ext}}^{\text{MP2}}}(\nu) - I_{TL_2^k}(\nu)$ (for $k = \{\text{HF}, \text{B3LYP}, \text{MP2}\}$) shown in the top panel of Figure 6 illustrate differences between TL₂^{HF}, TL₂^{B3LYP} and TL₂^{MP2} on the one hand and TL_{ext}^{MP2} as the reference. The smallest deviations are found for TL₂^{MP2}, as expected, while larger differences are found for TL^{HF} and TL^{B3LYP}. For example, the intensity of the peak at ~ 1620 cm⁻¹ is twice as large for TL₂^{HF} and the line positions of TL₂^{HF} and TL₂^{B3LYP} at ~ 1260 cm⁻¹ are shifted to the blue by ~ 3 cm⁻¹ compared to TL₂^{MP2} and TL_{ext}^{MP2}, respectively. The bottom panel shows the direct comparison of TL^{MP2} with the experimental spectrum determined in Reference 35 and illustrates the excellent agreement for frequencies between 500 and 1500 cm⁻¹. Somewhat larger deviations are found for peaks at ~ 1650 and 2900 cm⁻¹. Aside from obtaining correct peak positions from the calculated IR spectra, the infrared intensities are also found to remarkably well capture the trend visible in the experiment.

4 Discussion

The present study considered TL from a range of LL methods to CCSD(T) using variable amounts of HL information. For the molecule considered here - malonaldehyde - the relative computational cost of the LL methods ranged from 1 to $\sim 10^3$ but the qualities of the transfer-learned HL PESs - as inferred from the observables considered - were almost iden-

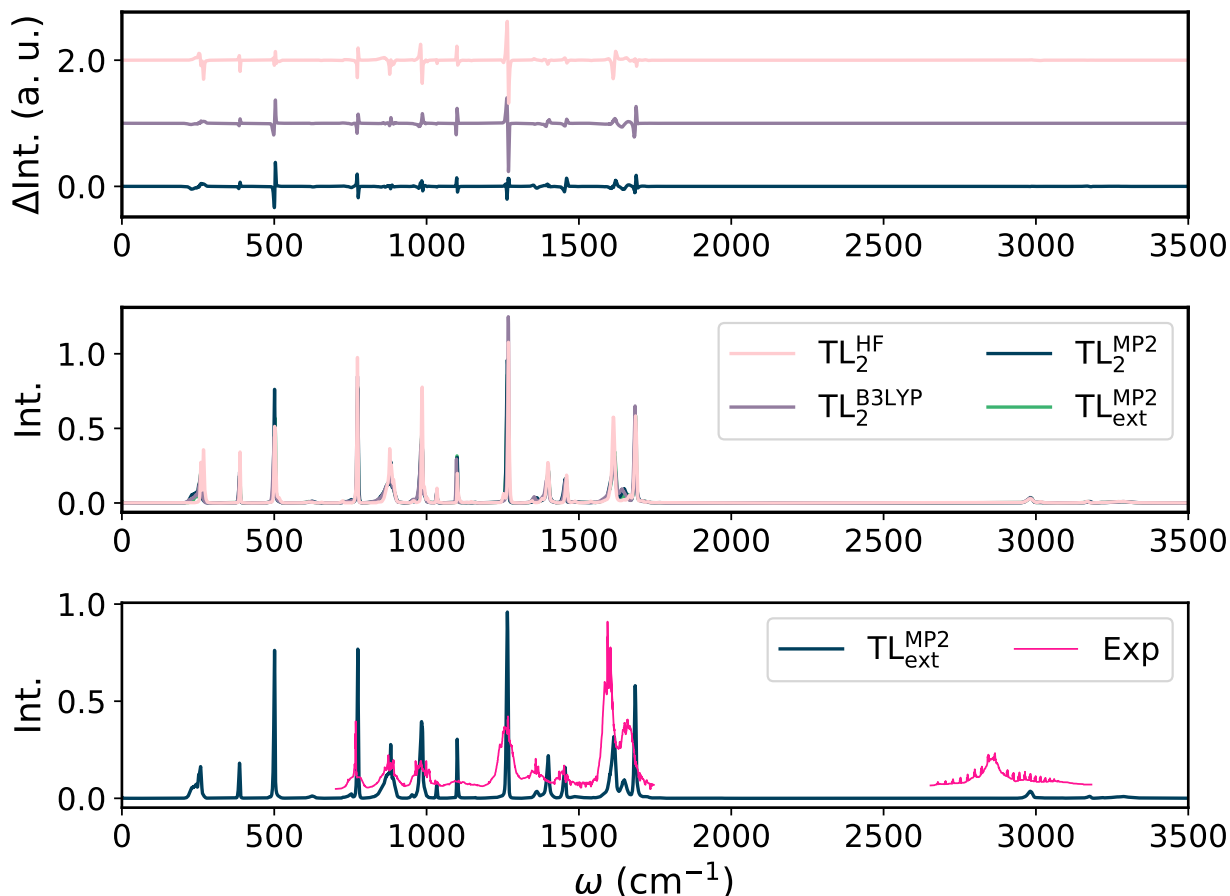


Figure 6: Infrared spectra calculated from finite- T MD simulations carried out on TL_2^{HF} , $\text{TL}_2^{\text{B3LYP}}$ and TL_2^{MP2} are shown in the middle panel. Each spectrum is averaged over 1000 independent trajectories of 250 ps and run with random momenta drawn from a Maxwell-Boltzmann distribution corresponding to 300 K. As comparison, an additional spectrum is determined from $\text{TL}_{\text{ext}}^{\text{MP2}}$ that has been trained on the extended data set containing 862 HL CCSD(T) points and serves as reference. All computed spectra are consistent among themselves and agree reasonably well. The top panel shows the difference spectra of TL_2^{HF} , $\text{TL}_2^{\text{B3LYP}}$ and TL_2^{MP2} with respect to $\text{TL}_{\text{ext}}^{\text{MP2}}$ which are shifted for clarity. The smallest overall differences are found for TL^{MP2} . The bottom panel shows the direct comparison of TL_2^{MP2} with the experimental spectrum determined in Reference 35 and illustrate the excellent agreement for frequencies between 500 and 1500 cm^{-1} . Somewhat larger deviations are found for peaks at ~ 1650 and 2900 cm^{-1} . Note that HCl impurities are observed at frequencies around 3000 cm^{-1} , see Reference 35 for details.

tical if 50 to 100 HL data points were used in the TL step. Two-dimensional projections of the LL PESs compared with the best HL target PES are reported in Figure 7. This provides a low-dimensional impression of the amount of reshaping that is conveyed by the TL step because all TL-PESs from the three LL reference calculations yield comparable final PESs.

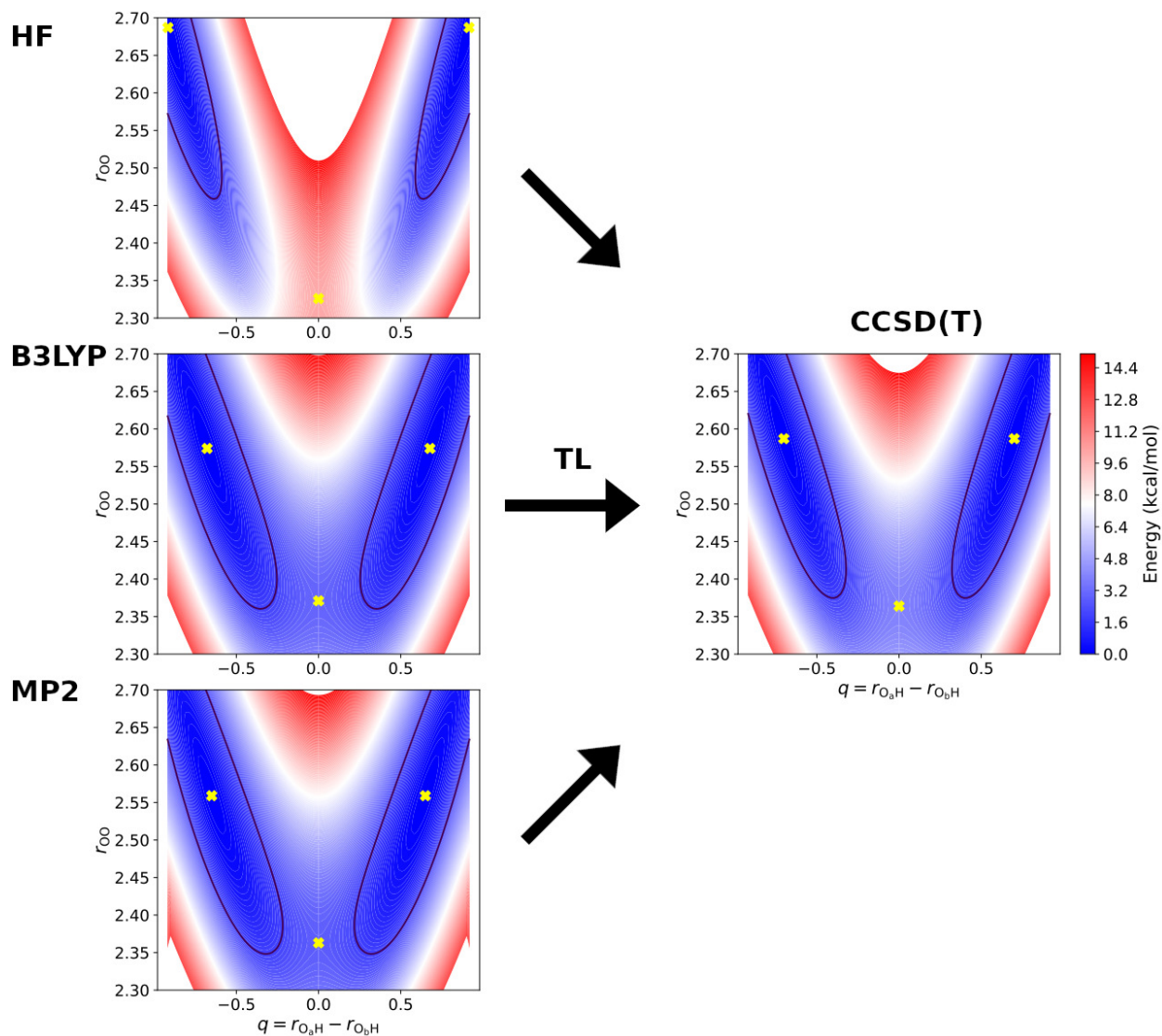


Figure 7: 2D representation of the LL (HF, B3LYP and MP2) and HL (TL with CCSD(T) target) PES spanned by the O–O distance and the reaction coordinate $q = r_{O_AH} - r_{O_BH}$. Isocontours of 2.0 kcal/mol are shown and the stationary points are marked by a gray cross.

Properties for which the performance of the transfer learned PESs were evaluated and compared included the barrier for H-transfer, the tunneling splittings, harmonic frequencies and IR spectra from finite-temperature MD simulations in the gas phase. All results suggest that the level of theory of the LL PES has only a minor influence on the quality of the resulting HL PES, although starting from a "better LL PES" (e.g. B3LYP/aVTZ) might have slight

advantages such as a shorter training time for TL. As an example, TL from PhysNet^{HF} to CCSD(T)/aVTZ based on 100 points required one order of magnitude more epochs than PhysNet^{B3LYP} or PhysNet^{MP2}. Thus, although transfer learning a surrogate model at the HF/aVDZ level yields a HL model of almost identical quality compared to TL₂^{B3LYP} and TL₂^{MP2}, the B3LYP/aVTZ level of theory may offer the best cost/accuracy ratio.

Starting from "equivalent" LL PESs in terms of representation error, a HL PESs of gold standard CCSD(T) quality was sought after and generated using TL. As an example for the performance of the TL step, normal mode frequencies are considered. The three LL PES achieve outstanding accuracy with respect to the frequencies from *ab initio* normal mode calculations at the respective levels of theory for both, the minimum energy structure and for the H-transfer transition state. PhysNet^{B3LYP} is most accurate with MAE(ω) = 2.6, RMSE(ω) = 3.5 cm⁻¹ and a maximum absolute error of \sim 8.7 cm⁻¹ for the global minimum of MA. This compares favourably with state of the art PESs for molecules of similar sizes. A recent permutationally invariant polynomial (PIP) PES for tropolone yields MAE(ω)^{min} between 1.7 and 12.7 cm⁻¹ the reported MAE(ω)^{TS} ranges from 8.4 cm⁻¹ to 18.6 cm⁻¹, depending on chosen PIP basis and other method-specific parameters.⁵⁹ PIP- and PhysNet-based PESs for the formic acid dimer find MAE(ω)^{min} of 14.9 and 6.4 cm⁻¹, respectively.⁶⁰⁻⁶² Comparing the harmonic frequencies from the LL PESs (HF, B3LYP and MP2) with the target level of theory, CCSD(T), reflects the amount of reshaping of the PES that is required in the TL step to reach the reported performance. This needs to be compared with differences in the harmonic frequencies at the *ab initio* HF/B3LYP/MP2 levels compared with the CCSD(T) frequencies³⁴ with an RMSE of 177, 28 and 21 cm⁻¹ for HF, B3LYP and MP2, respectively. TL with only 100 HL data points correctly reshaped the LL PESs with a MAE(ω) < 3 and RMSE(ω) < 4 cm⁻¹ (i.e. the same accuracy as for the most accurate LL PES, PhysNet^{B3LYP}, trained on several ten thousand structures), respectively, and impressively illustrates the data efficiency of TL. This translates into improvements of

1 to 2 orders of magnitude in accuracy for normal mode frequencies between reference and transfer-learned models

It is also valuable to consider the accuracy of the computed harmonic frequencies in light of the computational effort to obtain such frequencies (especially at the CCSD(T) level of theory) based on standard *ab initio* techniques. As is well established in the community, optimizations and frequency calculations at the CCSD(T) level of theory are tremendously time and resource intensive, especially for larger and complex systems. Starting from, e.g. PhysNet^{B3LYP}, required only 100 HL CCSD(T) data points (that include energies, forces and dipole moments) to achieve close to spectroscopic accuracy (i.e. more than 60 % of the frequencies with sub-1 cm⁻¹ accuracy and a maximum deviation of ~ 4 cm⁻¹ with respect to *ab initio* CCSD(T) reference). ML methods, especially in combination with data-efficient TL or related Δ -ML approaches, therefore offer an attractive time-saving alternative as has been demonstrated here. This is highlighted by recent *ab initio* LCCSD(T)-F12/cc-pVTZ-F12 calculations for 15-atom tropolone, for which the optimization and frequency calculation took 73 days on 12 cores.⁶³

The present findings underscore the importance for a sufficiently detailed LL model when aiming to construct a high-quality, versatile PES based on as little HL data as possible. This is shown by comparing to a model trained on the TL₂ (100 CCSD(T) data points) data set from scratch, i.e. without pre-training. The resulting model predicts the energy barrier moderately well (a deviation of ~ 0.05 kcal/mol with respect to reference), but has significantly larger errors for harmonic frequencies (i.e. $\text{MAE}(\omega) > 25$ cm⁻¹) than all TL_x_y models. In addition, starting MA structure optimization close to the stationary point is necessary for meaningful results. As anticipated, the attempt to run a MD simulation on such a PES fails entirely after a few time steps even at a rather low temperature of 300 K, which renders the PES unsuitable for dynamics studies.

Contrary to the model trained from scratch, TL enables to obtain a very HL representation of a global PES with very limited HL data points and, thus, allows to carry out dynamical assessments of a system. In this contribution this has been illustrated for the IR spectrum of MA and compared to experiment, for which good agreement is found. Since the TL data set contains only few structures which are chosen rather close to the global minimum and H-transfer transition state, it is conceivable that elevated temperatures lead to sampling structures with stronger distortions which are not fully covered by the TL data set. To the best of our knowledge, it is yet to be examined how a LL PES is transformed in regions where no TL data is supplied and presents a promising avenue for further investigation. Nevertheless, this very attractive route employing TL to obtain HL PESs allows CCSD(T)-quality MD simulations on the microsecond time scale for medium sized molecules. As an indication for the reduction in computing time achieved for MA it is noted that 1 ns of ML/MD simulation takes 12 CPU hours whereas the same simulation with *ab initio* MD simulations at the CCSD(T)/aVTZ level would take $2.2 \cdot 10^7$ hours, i.e. $\sim 2 \cdot 10^6$ longer, i.e. they are unfeasible. Of course such comparisons depend somewhat on the computer architecture and implementation used, but serve as an illustration that approaches as those discussed in the present work open possibilities to combine accuracy, system size and simulation lengths to approach CCSD(T)-level quality in sub μ s simulations that were unachievable with more established methods. With regards to PES generation, TL alleviates the problem of requiring thousands to tens of thousands of HL *ab initio* data points. This is a major step forward making highest levels of theory accessible. The adaptation of this approach to ML/MM simulations is a promising avenue towards stable, energy conserving, long-time quantitative condensed phase simulations.

5 Conclusion

The present work demonstrated that even with HF/aVDZ as the LL model high-quality full dimensional reactive PESs at the CCSD(T)/aVTZ level can be obtained through TL. Given a shape of the PES from a very economical level of theory, TL reshapes the LL PES to a HL PES from which observables agree favourable with both, experiments and models directly trained at the HL. Because the computational effort to evaluate energies and forces of a PES based on a NN does not depend on the level of *ab initio* theory used to conceive the representation, extensive and routine sub- μ s gas-phase ML//MD and condensed-phase ML/MM//MD simulations with the solvent treated with molecular mechanics become possible and are in reach.

Data Availability Statement

The MP2/aVTZ data set taken from previous work³³ is available on zenodo (<https://zenodo.org/record/3629239#.ZBh1J47MJH4>) and the PhysNet codes are available at <https://github.com/MMunibas/PhysNet>. Additional data sets generated during and/or analysed during the current study are available from the authors upon reasonable request.

Acknowledgments

The authors gratefully acknowledge partial financial support from the Swiss National Science Foundation through grant 200020_188724, the NCCR-MUST, and from the University of Basel.

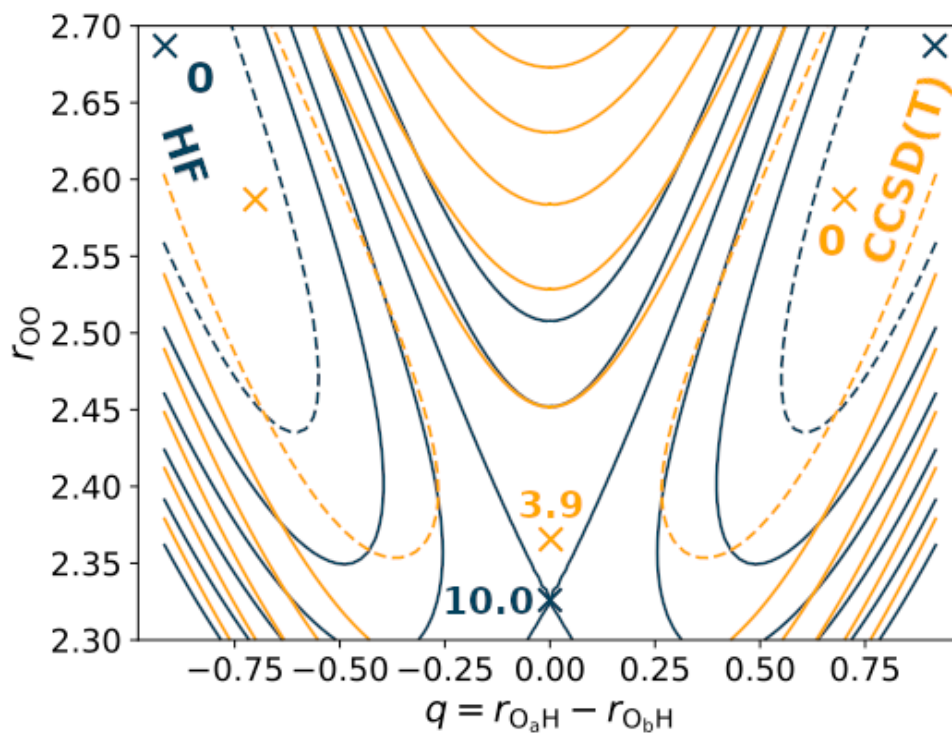


Figure 8: Table of contents graphic. Comparison of the LL HF/aVDZ (blue) and HL CCSD(T)/aVTZ (orange) PES with the dashed lines indicating the 2.5 kcal/mol isocontour.

References

- (1) Keith, J. A.; Vassilev-Galindo, V.; Cheng, B.; Chmiela, S.; Gastegger, M.; Müller, K.-R.; Tkatchenko, A. Combining machine learning and computational chemistry for predictive insights into chemical systems. *Chem. Rev.* **2021**, *121*, 9816–9872.
- (2) Meuwly, M. Machine learning for chemical reactions. *Chem. Rev.* **2021**, *121*, 10218–10239.
- (3) Unke, O. T.; Chmiela, S.; Sauceda, H. E.; Gastegger, M.; Poltavsky, I.; Schütt, K. T.; Tkatchenko, A.; Müller, K.-R. Machine learning force fields. *Chem. Rev.* **2021**, *121*, 10142–10186.
- (4) Coley, C. W.; Green, W. H.; Jensen, K. F. Machine learning in computer-aided synthesis planning. *Acc. Chem. Res.* **2018**, *51*, 1281–1289.
- (5) Chen, B.; Li, C.; Dai, H.; Song, L. Retro*: Learning Retrosynthetic Planning with Neural Guided A* Search. **2020**, *119*, 1608–1616.
- (6) Blaschke, T.; Arús-Pous, J.; Chen, H.; Margreitter, C.; Tyrchan, C.; Engkvist, O.; Papadopoulos, K.; Patronov, A. REINVENT 2.0: an AI tool for de novo drug design. *J. Chem. Inf. Model.* **2020**, *60*, 5918–5922.
- (7) Jiménez-Luna, J.; Grisoni, F.; Schneider, G. Drug discovery with explainable artificial intelligence. *Nat. Mach. Intell.* **2020**, *2*, 573–584.
- (8) Braams, B. J.; Bowman, J. M. Permutationally invariant potential energy surfaces in high dimensionality. *Int. Rev. Phys. Chem.* **2009**, *28*, 577–606.
- (9) Jiang, B.; Li, J.; Guo, H. Potential energy surfaces from high fidelity fitting of ab initio points: The permutation invariant polynomial-neural network approach. *Int. Rev. Phys. Chem.* **2016**, *35*, 479–506.

- (10) Käser, S.; Vazquez-Salazar, L. I.; Meuwly, M.; Töpfer, K. Neural network potentials for chemistry: concepts, applications and prospects. *Digital Discovery* **2023**, *2*, 28–58.
- (11) Manzhos, S.; Carrington Jr, T. Neural network potential energy surfaces for small molecules and reactions. *Chem. Rev.* **2020**, *121*, 10187–10217.
- (12) Vassilev-Galindo, V.; Fonseca, G.; Poltavsky, I.; Tkatchenko, A. Challenges for machine learning force fields in reproducing potential energy surfaces of flexible molecules. *J. Chem. Phys.* **2021**, *154*, 094119.
- (13) Ho, T.-S.; Rabitz, H. A general method for constructing multidimensional molecular potential energy surfaces from ab initio calculations. *J. Chem. Phys.* **1996**, *104*, 2584–2597.
- (14) Unke, O. T.; Meuwly, M. Toolkit for the construction of reproducing kernel-based representations of data: Application to multidimensional potential energy surfaces. *J. Chem. Inf. Model.* **2017**, *57*, 1923–1931.
- (15) Unke, O. T.; Meuwly, M. PhysNet: A neural network for predicting energies, forces, dipole moments, and partial charges. *J. Chem. Theory Comput.* **2019**, *15*, 3678–3693.
- (16) Schütt, K. T.; Sauceda, H. E.; Kindermans, P.-J.; Tkatchenko, A.; Müller, K.-R. SchNet—a deep learning architecture for molecules and materials. *J. Chem. Phys.* **2018**, *148*, 241722.
- (17) Hornik, K. Approximation capabilities of multilayer feedforward networks. *Neural Netw.* **1991**, *4*, 251–257.
- (18) Taylor, M. E.; Stone, P. Transfer learning for reinforcement learning domains: A survey. *J. Mach. Learn. Res.* **2009**, *10*, 1633–1685.
- (19) Smith, J. S.; Nebgen, B. T.; Zubatyuk, R.; Lubbers, N.; Devereux, C.; Barros, K.; Tretiak, S.; Isayev, O.; Roitberg, A. E. Approaching coupled cluster accuracy with

- a general-purpose neural network potential through transfer learning. *Nat. Commun.* **2019**, *10*, 1–8.
- (20) Pan, S. J.; Yang, Q. A survey on transfer learning. *IEEE Trans. Knowl. Data Eng.* **2009**, *22*, 1345–1359.
- (21) Firth, D.; Beyer, K.; Dvorak, M.; Reeve, S.; Grushow, A.; Leopold, K. Tunable far-infrared spectroscopy of malonaldehyde. *J. Chem. Phys.* **1991**, *94*, 1812–1819.
- (22) Baba, T.; Tanaka, T.; Morino, I.; Yamada, K. M.; Tanaka, K. Detection of the tunneling-rotation transitions of malonaldehyde in the submillimeter-wave region. *J. Chem. Phys.* **1999**, *110*, 4131–4133.
- (23) Baughcum, S. L.; Smith, Z.; Wilson, E. B.; Duerst, R. W. Microwave spectroscopic study of malonaldehyde. 3. Vibration-rotation interaction and one-dimensional model for proton tunneling. *J. Am. Chem. Soc.* **1984**, *106*, 2260–2265.
- (24) Turner, P.; Baughcum, S. L.; Coy, S. L.; Smith, Z. Microwave spectroscopic study of malonaldehyde. 4. Vibration-rotation interaction in parent species. *J. Am. Chem. Soc.* **1984**, *106*, 2265–2267.
- (25) Smith, Z.; Wilson, E. B.; Duerst, R. W. The infrared spectrum of gaseous malonaldehyde (3-hydroxy-2-propenal). *Spectrochim. Acta A* **1983**, *39*, 1117–1129.
- (26) Firth, D. W.; Barbara, P. F.; Trommsdorff, H. P. Matrix induced localization of proton tunneling in malonaldehyde. *Chem. Phys.* **1989**, *136*, 349–360.
- (27) Chiavassa, T.; Roubin, P.; Pizzala, L.; Verlaque, P.; Allouche, A.; Marinelli, F. Experimental and theoretical studies of malonaldehyde: Vibrational analysis of a strongly intramolecularly hydrogen bonded compound. *J. Phys. Chem.* **1992**, *96*, 10659–10665.
- (28) Duan, C.; Luckhaus, D. High resolution IR-diode laser jet spectroscopy of malonaldehyde. *Chem. Phys. Lett.* **2004**, *391*, 129–133.

- (29) Wang, Y.; Braams, B. J.; Bowman, J. M.; Carter, S.; Tew, D. P. Full-dimensional quantum calculations of ground-state tunneling splitting of malonaldehyde using an accurate ab initio potential energy surface. *J. Chem. Phys.* **2008**, *128*, 224314.
- (30) Yang, Y.; Meuwly, M. A generalized reactive force field for nonlinear hydrogen bonds: Hydrogen dynamics and transfer in malonaldehyde. *J. Chem. Phys.* **2010**, *133*, 064503.
- (31) Mizukami, W.; Habershon, S.; Tew, D. P. A compact and accurate semi-global potential energy surface for malonaldehyde from constrained least squares regression. *J. Chem. Phys.* **2014**, *141*, 144310.
- (32) Huang, J.; Buchowiecki, M.; Nagy, T.; Vaníček, J.; Meuwly, M. Kinetic isotope effect in malonaldehyde determined from path integral Monte Carlo simulations. *Phys. Chem. Chem. Phys.* **2014**, *16*, 204–211.
- (33) Käser, S.; Unke, O. T.; Meuwly, M. Reactive dynamics and spectroscopy of hydrogen transfer from neural network-based reactive potential energy surfaces. *New J. Phys.* **2020**, *22*, 055002.
- (34) Käser, S.; Richardson, J. O.; Meuwly, M. Transfer Learning for Affordable and High-Quality Tunneling Splittings from Instanton Calculations. *J. Chem. Theory Comput.* **2022**, *18*, 6840–6850.
- (35) Lüttschwager, N. O.; Wassermann, T. N.; Coussan, S.; Suhm, M. A. Vibrational tuning of the Hydrogen transfer in malonaldehyde—a combined FTIR and Raman jet study. *Mol. Phys.* **2013**, *111*, 2211–2227.
- (36) Gilmer, J.; Schoenholz, S. S.; Riley, P. F.; Vinyals, O.; Dahl, G. E. Neural message passing for quantum chemistry. Proc. of the 34th Int. Conf. on Machine Learning—Volume 70. 2017; pp 1263–1272.

- (37) Baydin, A. G.; Pearlmutter, B. A.; Radul, A. A.; Siskind, J. M. Automatic differentiation in machine learning: a survey. *J. Mach. Learn. Res.* **2017**, *18*, 5595–5637.
- (38) Abadi, M.; Barham, P.; Chen, J.; Chen, Z.; Davis, A.; Dean, J.; Devin, M.; Ghemawat, S.; Irving, G.; Isard, M. et al. Tensorflow: A system for large-scale machine learning. 12th USENIX symposium on operating systems Design and Implementation (OSDI 16). 2016; pp 265–283.
- (39) Tan, C.; Sun, F.; Kong, T.; Zhang, W.; Yang, C.; Liu, C. A survey on deep transfer learning. International conference on artificial neural networks. 2018; pp 270–279.
- (40) Fu, B.; Xu, X.; Zhang, D. H. A hierarchical construction scheme for accurate potential energy surface generation: An application to the F+ H₂ reaction. *J. Chem. Phys.* **2008**, *129*, 011103.
- (41) Ramakrishnan, R.; Dral, P.; Rupp, M.; von Lilienfeld, O. A. Big Data meets quantum chemistry approximations: The Δ -machine learning approach. *J. Chem. Theory Comput.* **2015**, *11*, 2087–2096.
- (42) Bowman, J. M.; Qu, C.; Conte, R.; Nandi, A.; Houston, P. L.; Yu, Q. Δ -Machine Learned Potential Energy Surfaces and Force Fields. *J. Chem. Theory Comput.* **2023**, *19*, 1–17.
- (43) Huang, B.; von Lilienfeld, O. A. Quantum machine learning using atom-in-molecule-based fragments selected on the fly. *Nat. Chem.* **2020**, *12*, 945–951.
- (44) Stewart, J. J. Optimization of parameters for semiempirical methods V: Modification of NDDO approximations and application to 70 elements. *J. Mol. Model.* **2007**, *13*, 1173–1213.
- (45) J.J.P. Stewart, S. C. C. MOPAC 2016. 2016; Colorado Springs, CO, USA.

- (46) Werner, H.-J.; Knowles, P. J.; Knizia, G.; Manby, F. R.; Schütz, M.; Celani, P.; Györffy, W.; Kats, D.; Korona, T.; Lindh, R. et al. MOLPRO, version 2021, a package of ab initio programs. 2019.
- (47) Csányi, G.; Albaret, T.; Payne, M.; De Vita, A. “Learn on the fly”: A hybrid classical and quantum-mechanical molecular dynamics simulation. *Phys. Rev. Lett.* **2004**, *93*, 175503.
- (48) Richardson, J. O.; Althorpe, S. C. Ring-polymer instanton method for calculating tunneling splittings. *J. Chem. Phys.* **2011**, *134*, 054109.
- (49) Richardson, J. O. Ring-polymer instanton theory. *Int. Rev. Phys. Chem.* **2018**, *37*, 171–216.
- (50) Richardson, J. O.; Pérez, C.; Lobsiger, S.; Reid, A. A.; Temelso, B.; Shields, G. C.; Kisiel, Z.; Wales, D. J.; Pate, B. H.; Althorpe, S. C. Concerted Hydrogen-Bond Breaking by Quantum Tunneling in the Water Hexamer Prism. *Science* **2016**, *351*, 1310–1313.
- (51) Richardson, J. O. Full-and reduced-dimensionality instanton calculations of the tunnelling splitting in the formic acid dimer. *Phys. Chem. Chem. Phys.* **2017**, *19*, 966–970.
- (52) Mil’nikov, G. V.; Nakamura, H. Practical implementation of the instanton theory for the ground-state tunneling splitting. *J. Chem. Phys.* **2001**, *115*, 6881–6897.
- (53) Richardson, J. O.; Althorpe, S. C. Ring-polymer instanton method for calculating tunneling splittings. *J. Chem. Phys.* **2011**, *134*, 054109.
- (54) Richardson, J. O. Ring-polymer instanton theory. *Intern. Rev. Phys. Chem.* **2018**, *37*, 171–216.
- (55) Larsen, A. H.; Mortensen, J. J.; Blomqvist, J.; Castelli, I. E.; Christensen, R.; Dułak, M.; Friis, J.; Groves, M. N.; Hammer, B.; Hargus, C. et al. The atomic simula-

- tion environment – a Python library for working with atoms. *J. Phys. Condens. Matter* **2017**, *29*, 273002.
- (56) Meuwly, M.; Karplus, M. Simulation of proton transfer along ammonia wires: An “ab initio” and semiempirical density functional comparison of potentials and classical molecular dynamics. *J. Chem. Phys.* **2002**, *116*, 2572–2585.
- (57) Töpfer, K.; Koner, D.; Erramilli, S.; Ziegler, L. D.; Meuwly, M. Molecular-Level Understanding of the Ro-vibrational Spectra of N₂O in Gaseous, Supercritical and Liquid SF₆ and Xe. *arXiv preprint arXiv:2302.07179* **2023**,
- (58) Kumar, P.; Marx, D. Quantum corrections to classical time-correlation functions: Hydrogen bonding and anharmonic floppy modes. *J. Chem. Phys.* **2004**, *121*, 9.
- (59) Houston, P.; Conte, R.; Qu, C.; Bowman, J. M. Permutationally invariant polynomial potential energy surfaces for tropolone and H and D atom tunneling dynamics. *J. Chem. Phys.* **2020**, *153*, 024107.
- (60) Qu, C.; Bowman, J. M. An ab initio potential energy surface for the formic acid dimer: zero-point energy, selected anharmonic fundamental energies, and ground-state tunneling splitting calculated in relaxed 1–4-mode subspaces. *Phys. Chem. Chem. Phys.* **2016**, *18*, 24835–24840.
- (61) Käser, S.; Boittier, E. D.; Upadhyay, M.; Meuwly, M. Transfer Learning to CCSD(T): Accurate Anharmonic Frequencies from Machine Learning Models. *J. Chem. Theory Comput.* **2021**, *17*, 3687–3699.
- (62) Käser, S.; Meuwly, M. Transfer learned potential energy surfaces: accurate anharmonic vibrational dynamics and dissociation energies for the formic acid monomer and dimer. *Phys. Chem. Chem. Phys.* **2022**, *24*, 5269–5281.

- (63) Qu, C.; Houston, P. L.; Conte, R.; Nandi, A.; Bowman, J. M. Breaking the coupled cluster barrier for machine-learned potentials of large molecules: The case of 15-atom acetylacetone. *J. Phys. Chem. Lett.* **2021**, *12*, 4902–4909.

Supporting Information: Transfer-Learned Potential Energy Surfaces: Towards Microsecond -Scale Molecular Dynamics Simulations in the Gas Phase at CCSD(T) Quality

March 22, 2023

Table S1: Harmonic frequencies of MA determined from PhysNet trained on different level of theory data and their comparison to the respective reference. Frequencies are given in cm^{-1} . The mean average and root mean squared (MAE and RMSE) errors between the frequencies determined from the NN and direct *ab initio* calculations at the respective level of theory are given in the last two lines. A corresponding table for the frequencies of the H-transfer TS is given in Tab. S2.

Mode	PhysNet ^{HF}	HF	PhysNet ^{B3LYP}	B3LYP	PhysNet ^{MP2}	MP2
1	260.2	258.1	288.9	280.2	277.8	277.5
2	277.9	267.9	289.9	287.7	294.7	286.6
3	433.8	424.9	400.9	402.2	393.8	394.3
4	529.9	529.2	521.2	521.6	512.7	514.1
5	820.0	823.6	789.3	789.6	787.9	789.4
6	853.9	858.2	896.1	894.6	888.7	888.6
7	958.9	957.9	941.8	944.3	937.6	937.6
8	1029.8	1032.5	1002.8	1002.1	1016.9	1012.3
9	1118.3	1119.5	1025.8	1024.5	1025.0	1023.8
10	1162.9	1161.9	1048.4	1048.8	1049.8	1048.8
11	1207.7	1201.2	1120.0	1116.6	1118.0	1109.7
12	1352.4	1369.1	1279.5	1286.8	1289.5	1288.3
13	1505.8	1503.3	1389.8	1388.0	1405.1	1403.1
14	1522.9	1519.6	1405.2	1405.0	1413.5	1408.0
15	1578.2	1585.4	1480.9	1478.9	1478.6	1482.1
16	1786.8	1776.6	1627.7	1624.4	1640.4	1641.5
17	1930.7	1930.6	1696.2	1692.1	1692.8	1692.9
18	3158.3	3163.2	2968.9	2966.7	3037.1	3039.0
19	3354.5	3359.1	3106.7	3101.1	3114.4	3107.1
20	3384.8	3387.3	3175.9	3171.3	3216.5	3217.9
21	3896.8	3890.6	3212.8	3214.0	3269.1	3267.3
MAE	4.8		2.6		2.5	
RMSE	6.2		3.5		3.6	

Table S2: Harmonic frequencies of the H-transfer TS of MA determined from PhysNet trained on different level of theory data and their comparison to the respective reference. The mean average and root mean squared (MAE and RMSE) errors between the frequencies determined from the NN and direct *ab initio* calculations at the respective level of theory are given in the last two lines. Frequencies are given in cm^{-1} .

Mode	PhysNet ^{HF}	HF	PhysNet ^{B3LYP}	B3LYP	PhysNet ^{MP2}	MP2
i	1761.0	1764.2	1186.0	1177.8	1193.3	1167.7
2	396.2	394.9	369.4	369.8	373.7	373.0
3	419.0	414.3	398.4	397.1	379.3	377.2
4	619.4	618.2	576.5	576.0	562.4	567.3
5	653.2	675.7	616.7	617.9	618.2	622.9
6	817.3	812.0	783.8	785.1	786.4	787.7
7	1025.8	1027.7	947.5	948.1	937.9	943.0
8	1125.8	1126.8	1001.0	1002.4	994.0	992.3
9	1141.1	1136.2	1049.8	1048.9	1051.6	1052.2
10	1178.4	1181.6	1059.0	1060.4	1072.9	1072.6
11	1198.7	1185.0	1110.9	1112.4	1113.1	1106.8
12	1412.2	1406.1	1293.3	1295.7	1304.0	1301.7
13	1417.0	1415.5	1329.9	1332.9	1340.3	1341.4
14	1480.5	1483.9	1370.3	1371.5	1381.4	1378.9
15	1611.0	1615.9	1507.0	1505.6	1505.5	1510.0
16	1736.7	1737.6	1608.3	1611.4	1646.2	1646.8
17	1819.0	1813.5	1633.6	1633.6	1666.6	1669.6
18	2057.1	2046.2	1891.2	1879.3	1890.0	1866.4
19	3284.7	3280.6	3080.3	3080.1	3137.4	3140.1
20	3287.8	3281.2	3083.1	3080.4	3141.0	3140.8
21	3410.3	3409.8	3234.5	3230.2	3291.3	3282.2
MAE	5.1		2.3		4.9	
RMSE	7.2		3.6		8.4	

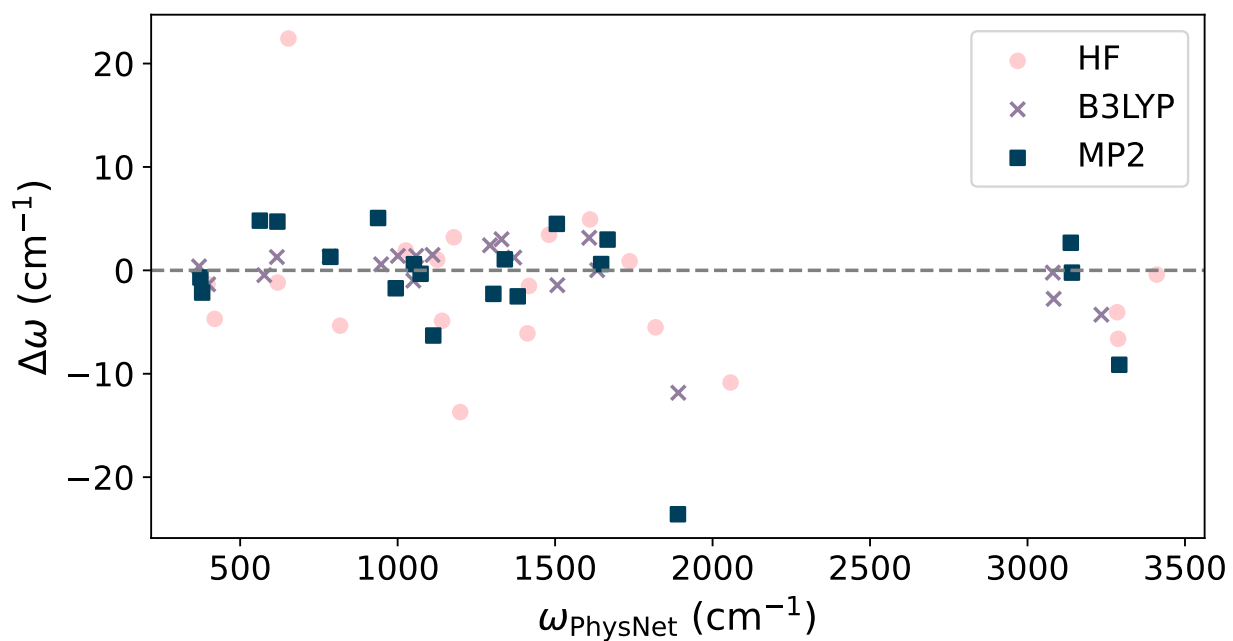


Figure S1: Harmonic frequencies of the H-transfer TS of MA determined from PhysNet trained on different level of theory data and their comparison to the respective reference. Here, $\Delta\omega = \omega_{\text{Ref.}} - \omega_{\text{PhysNet}}$.